Author Manuscript

Author Manuscript

Author Manuscript

Author Manuscript

HHS Public Access

Author manuscript

J Am Chem Soc. Author manuscript; available in PMC 2026 June 05.

Published in final edited form as:

J Am Chem Soc. 2026 May 27; 148(20): 20322–20327. doi:10.1021/jacs.5c21227.

Ribosome Heterogeneity Revealed by Complex-Up Native Mass Spectrometry and Top-Down Proteomics

Sachin C. Tennakoon,

Department of Chemistry, University of Nebraska-Lincoln, Lincoln, Nebraska 68588, United States

Sarah B. Giese,

Coe College, Cedar Rapids, Iowa 52402, United States

Jared B. Shaw

Department of Chemistry, University of Nebraska-Lincoln, Lincoln, Nebraska 68588, United States

Abstract

Characterization of large molecular machines, such as the ribosome, under a breadth of biological states to elucidate regulatory details remains challenging. Herein, a workflow combining complex-up native mass spectrometry (nMS) with infrared multiphoton dissociation (IRMPD) and top-down proteomics (TDP) was developed to enable the rapid and direct characterization of ribosome heterogeneity. Preferential unfolding and fragmentation of rRNA by IRMPD enabled proteoform-resolved characterization of *E. coli* ribosome heterogeneity across growth states revealing ribosomal protein (RP) heterogeneity in unprecedented detail. TDP characterization of isolated RPs enabled confident proteoform characterization and facile interpretation of the IRMPD spectra. Additionally, differences in proteoform relative abundances determined by complex-up nMS and TDP reveal proteoform specific changes in relative interaction strengths. This experimental framework paves the way to a more rapid understanding of the diverse regulatory mechanisms conferred by ribonucleoprotein heterogeneity, including the role of RP composition and post-translational modification (PTM) heterogeneity in modulation of translation efficiency and specificity.

Precise temporal and spatial control of protein expression via regulation of the translation machinery is critical to cellular energy conservation and adaptation to environmental stresses.[1] Emerging evidence suggests heterogeneity in ribosome composition provides enhanced regulatory capacity in the form of specialized compositions that, for example, yield preference for specific mRNAs, modulate translation speed and accuracy, and ribosome subcellular localization.[2-7] Sources of heterogeneity include ribosomal RNA

This article is licensed under CC-BY-NC-ND 4.0

Corresponding Author Department of Chemistry, University of Nebraska–Lincoln, Lincoln, Nebraska 68588, United States; jshaw17@unl.edu.

Author Contributions

The manuscript was written through contributions of all authors. All authors have given approval to the final version of the manuscript.

The authors declare no competing financial interest.

Author Manuscript Author Manuscript Author Manuscript Author Manuscript

(rRNA) sequence and modifications, RP stoichiometry and PTMs, and ribosome-associated proteins (RAPs). Native mass spectrometry has emerged as a powerful tool for probing the structure and composition of macromolecular assemblies and informing high-resolution structure determination.[8-10] Landmark publications from Robinson and co-workers demonstrated the utility of nMS measurements of the ribosome and its subunits[11-13] for greater mechanistic understanding.[14-18] Additionally, recent advances in instrumentation dedicated to nMS have enabled Heck and co-workers to measure large biomolecular assemblies, including the ribosome, with unprecedented resolution, accuracy, and sensitivity.[19-22] While nMS generally provides putative identification of assemblies, subcomplexes, and subunits based on intact masses, TDP enables direct characterization of subunit proteoforms[23] for determination of primary structure and combinatorial modifications.[24,25] Recent studies have highlighted the advantages of integrating TDP into workflows to achieve more extensive characterization of RPs, subcomplexes, and cation binding sites.[26-28] Despite these advances in the measurement of intact ribosomal assemblies and characterization of ribosomal proteins, limited progress has been made to enable direct elucidation of heterogeneity at the assembly level.

Here, we present the development of a combined approach using complex-up[29] nMS with IRMPD and TDP as a powerful framework for dissecting ribosome heterogeneity. IRMPD yielded efficient dissociation of intact 30S and 50S subunits of *E. coli* ribosomes via preferential unfolding and fragmentation of the rRNA to liberate abundant RPs and RAPs. Proteoform characterization by TDP combined with complex-up nMS revealed ribosome heterogeneity in exquisite detail and provides a new approach to proteoform-resolved relative interaction strengths.

Top-down proteomics was first performed to characterize the proteoforms present in *E. coli* strain B ribosomes (Table S1). High-resolution nMS measurements of the intact 30S and 50S subunits (Figure 1A) contain baseline-resolved charge states that reveal three major species for each subunit. The most abundant 30S subunit species correspond to the complete 30S subunit plus stationary-phase-induced ribosome-associated protein (SRA) and the 30S subunit containing the addition of SRA and the loss of S1. A minor species also shows the loss of S1 and S2. These observations are supported by the substoichiometric ratio of S1 due to its weak and reversible association with the 30S subunit and additional nonribosomal functions.[30-32] The most abundant 50S subunit species corresponds to the intact 50S subunit. Two additional abundant 50S subunit species were observed that correspond to the complete loss of the $L10(L7/L12_2)_2$ stalk complex and the loss of L1 with addition of the RAP RsfS (ribosome silencing factor RsfS). Despite the high quality of the intact mass measurements of the 30S and 50S subunits, a significant degree of heterogeneity in the form of combinatorial subunit composition, RP PTMs, rRNA modifications, cation binding, etc., is masked within the charge state distributions of these state-of-the-art measurements.

As a large ribonucleoprotein complex, the distinct chemical properties of the rRNA and protein components of the ribosome were exploited to enable efficient subunit dissociation. Our hypothesis was that IRMPD would yield preferential unfolding and fragmentation of the rRNA accompanied by the efficient release of intact RPs and RAPs. Previous studies have shown that the P—O bonds in phosphorylated polypeptides and oligonucleotides are strong

Author Manuscript Author Manuscript Author Manuscript Author Manuscript

chromophores for 10.6 μm photons. Additionally, DNA/RNA fragment more readily than phosphorylated polypeptides due to phosphodiester bonds between every residue, yielding far greater absorption cross sections.[33,34] Experimental parameters under which covalent bond cleavage was only expected for rRNA were refined using model phosphorylated peptides/proteins and RNAs (Figures S1 and S2).

Figure 1B and 1C show complex-up nMS IRMPD spectra of mass selected 30S and 50S ribosomal subunits, respectively. IRMPD yielded near complete dissociation of both 30S and 50S subunits and extensive release of the constituent RPs and RAPs. The low m/z regions of the IRMPD spectra are dominated by abundant charge state distributions of the ejected proteins, and ultrahigh resolving power mass analysis enabled facile charge deconvolution and monoisotopic mass determination (inset panels of Figure 1B and C). The determined masses were assigned to RPs and RAPs with mass errors less than 2 ppm based on proteoforms determined by TDP. Annotation of the IRMPD spectra immediately revealed heterogeneity in RP PTMs, truncated RPs, and confirmed the presence of the RsfS. Another striking characteristic of the IRMPD spectra is evidence for asymmetric charge partitioning in the released RPs and RAPs resulting from the slow heating induced by IRMPD.[35,36] The high charge and low m/z of the released proteins indicate the possibility of significant vibrational energy transfer from the rRNA to the proteins in addition to direct photon absorption by proteins during the 10–40 ms process. Overall, IRMPD liberated greater than 60% of the core 30S and 50S ribosomal proteins and the RAP RsfS (Figures S3, S4).

Figure 2 shows structures of 30S and 50S subunits with the proteins observed in the IRMPD spectra highlighted in red. To rationalize which RPs and RAPs were observed and the relative intensities of the observed proteins, we examined the interface surface areas of the proteins in available high-resolution structures of free 30S and 50S subunits. For the 50S subunit, we found the fraction of protein surface area involved in interfaces to be a reasonable predictor of observation and relative abundance. Tables S2 and S3 contain parameters related to the interaction of RPs with rRNA and other RPs, such as surface area, hydrogen bonds, etc., calculated using PDBe PISA v1.52. For example, L9 was one of the most abundant proteins observed in the IRMPD spectrum of the 50S subunit (Figure 1C) along with loosely associated stalk complex proteins L7, L12, and L10. This intuitively makes sense due to L9 association with the 23S rRNA via a small interface, 4.9% of total surface area of L9, at the end of its elongated structure, as seen in Figure 2B. Of the 13 50S RPs observed in IRMPD and in the crystal structure, ten of them had interface surface areas corresponding to less than 35% of their total surface area. Contrarily, RPs L34 and L35 are buried within the folds of the 23S rRNA tertiary structure and have fractional interface surface areas of 55% and 47%, respectively. Observation of these RPs would require significant unfolding of the 23S rRNA. Interestingly, RP L20 was observed in the IRMPD spectra, despite having the largest fractional interface surface area, 56%. The elongated helical structure of the N-terminal portion of L20 is enveloped by folds of the 23S rRNA. However, these folds are at the surface of the 50S subunit and likely more readily disrupted to enable the release of L20 from the complex. Protein appearance energies and intensities from energy-resolved IRMPD experiments (Figure S5) further illustrate the sensitivity of IRMPD to subunit interface area and interaction strength.

Author Manuscript Author Manuscript Author Manuscript Author Manuscript

To demonstrate the utility of our combined nMS and TDP approach, we characterized ribosomes isolated from *E. coli* strain K12 grown to mid-log, late-log, and stationary phase by complex-up nMS and TDP. Native mass spectra of the intact 30S and 50S subunits and IRMPD spectra of the mass selected subunits are provided in Figures S6 and S7. Efficient and extensive dissociation of the subunits by IRMPD enabled a comparison of RP proteoform relative abundances at different growth phases (Figure 3). Although the exact function of C-terminal glutamylation of S6 is unknown, it is well-established that the extent of glutamylation changes only during stationary phase in *E. coli*.[37] The intensity-weighted number of C-terminal glutamylation was 0.755 ± 0.003, 0.726 ± 0.005, and 1.828 ± 0.008 for mid-log, late-log, and stationary phase, respectively, and is in agreement with previous studies. Similarly, the L7:L12 ratio is known to increase during the course of cell growth via exchange of L12 and L7 (N-terminal-acetylated L12) monomers within the $L10(L7/L12_2)_2$ stalk complex.[16,38] We observed L7:L12 ratios of 2.15:1, 4.29:1, and 14.0:1 for ribosomes isolated from cell cultures in mid-log, late-log, and stationary phase, respectively. This is consistent with understanding that N-terminal acetylation tightens interactions with L10 to increase the stability of the stalk complex during stationary phase.[16,39] These results were compared to proteoform relative abundances determined by TDP (Table S4) to further investigate the accuracy of proteoform relative abundances determined by complex-up nMS with IRMPD.

Strong agreement was observed between complex-up IRMPD and TDP on the intensity-weighted number of C-terminal glutamylation on S6 and L7/L12 compositions, except in one case. The C-terminus of S6 does not interact with other components of the ribosome. Consequently, a high degree of agreement is expected and observed for all S6 proteoforms during all phases of cell growth (Figure 4A). TDP is expected to give “true” proteoform relative abundances, because the analysis is performed under denaturing conditions w onne qu cromaograpy separation of the proteins. However, variations in interactions of the RPs, perhaps modulated by PTMs, with rRNA or other RPs are expected to impact proteoform abundances observed in complex-up nMS analysis due to varying strengths of interactions within the assembly.

This is highlighted by the marked difference in the L7:L12 ratio (49:1 by TDP compared to 14:1 by complex-up IRMPD) determined during the stationary phase (OD 1.37, Figure 4B). As discussed above, N-terminal acetylation in L7 is known to stabilize interactions between the N-terminal domain of L7 and L10, the anchoring point of the stalk to the 50S subunit. The underestimation of L7 abundance by complex-up nMS with IRMPD is attributed to the increased stability of the L7-rich stalk complex and reduced yield of L7 monomers in the IRMPD spectra. In the context of translation down-regulation during stationary phase, a more rigid stalk complex may reduce efficiency of translation factor recruitment and represent one of the many likely concomitant mechanisms for reducing translation efficiency. Additionally, these results illustrate the potential for the combination of complex-up nMS with IRMPD and TDP determined RP relative abundances to provide proteoform-resolved interaction strengths in the context of very large, heterogeneous assemblies. This is specificity that might only be attainable by native mass spectrometry.

Author Manuscript Author Manuscript Author Manuscript Author Manuscript

In summary, we developed a combined complex-up nMS and TDP workflow for direct characterization of ribosome heterogeneity using *E. coli* as a model system. However, the methodology is completely transferable to eukaryotic and archaeal ribosomes and is applicable to ribonucleoproteins in general. We envision this approach playing a critical role in characterization of ribonucleoprotein composition and discovery of associated proteins, e.g., new classes of ribosome hibernation factors,[40] as well as providing critical biophysical information that links specific proteoforms to regulatory mechanisms.

Supplementary Material

Refer to Web version on PubMed Central for supplementary material.

ACKNOWLEDGMENTS

This work is supported by the National Institutes of Health (R35GM157097), Nebraska Center for Integrated Biomolecular Communication (P20GM113126), and startup funds from the University of Nebraska–Lincoln. S.B.G. was supported by the National Science Foundation Research Experience for Undergraduates program (CHE2447813).

Data Availability Statement

The raw MS data and identifications for top-down proteomics analyses are available on ProteomeXchange with data set identifiers PXD069930 and PXD069929. Native MS data are available on MassIVE with data set identifiers MSV000100578 and MSV000100579.

REFERENCES

(1). Xue S; Barna M Specialized Ribosomes: A New Frontier in Gene Regulation and Organismal Biology. Nat. Rev. Mol. Cell Biol 2012, 13 (6), 355–369. [PubMed: 22617470]

(2). Sauert M; Temmel H; Moll I Heterogeneity of the Translational Machinery: Variations on a Common Theme. Biochimie 2015, 114, 39–47. [PubMed: 25542647]

(3). Simsek D; Barna M An Emerging Role for the Ribosome as a Nexus for Post-Translational Modifications. Curr. Opin Cell Biol 2017, 45, 92–101. [PubMed: 28445788]

(4). Genuth NR; Barna M The Discovery of Ribosome Heterogeneity and Its Implications for Gene Regulation and Organismal Life. Mol. Cell 2018, 71 (3), 364–374. [PubMed: 30075139]

(5). Segev N; Gerst JE Specialized Ribosomes and Specific Ribosomal Protein Paralogs Control Translation of Mitochondrial Proteins. J. Cell Biol 2018, 217 (1), 117–126. [PubMed: 29118025]

(6). Emmott E; Jovanovic M; Slavov N Ribosome Stoichiometry: From Form to Function. Trends Biochem. Sci 2019, 44 (2), 95–109. [PubMed: 30473427]

(7). Gay DM; Lund AH; Jansson MD Translational Control through Ribosome Heterogeneity and Functional Specialization. Trends Biochem. Sci 2022, 47 (1), 66–81. [PubMed: 34312084]

(8). Mehmood S; Allison TM; Robinson CV Mass Spectrometry of Protein Complexes: From Origins to Applications. Annu. Rev. Phys. Chem 2015, 66 (1), 453–474. [PubMed: 25594852]

(9). Leney AC; Heck AJR Native Mass Spectrometry: What Is in the Name? J. Am. Soc. Mass Spectrom 2017, 28 (1), 5–13.

(10). Jooß K; McGee JP; Kelleher NL Native Mass Spectrometry at the Convergence of Structural Biology and Compositional Proteomics. Acc. Chem. Res 2022, 55 (14), 1928–1937. [PubMed: 35749283]

(11). Rostom AA; Fucini P; Benjamin DR; Juenemann R; Nierhaus KH; Hartl FU; Dobson CM; Robinson CV Detection and Selective Dissociation of Intact Ribosomes in a Mass Spectrometer. Proc. Natl. Acad. Sci. U. S. A 2000, 97 (10), 5185–5190. [PubMed: 10805779]

Author Manuscript Author Manuscript Author Manuscript Author Manuscript

(12). Videler H; Ilag LL; McKay ARC; Hanson CL; Robinson CV Mass Spectrometry of Intact Ribosomes. FEBS Lett, 2005, 579 (4), 943–947. [PubMed: 15680979]

(13). McKay AR; Ruotolo BT; Ilag LL; Robinson CV Mass Measurements of Increased Accuracy Resolve Heterogeneous Populations of Intact Ribosomes. J. Am. Chem. Soc 2006, 128 (35), 11433–11442. [PubMed: 16939266]

(14). Hanson CL; Fucini P; Ilag LL; Nierhaus KH; Robinson CV Dissociation of Intact Escherichia Coli Ribosomes in a Mass Spectrometer: Evidence for Conformational Change in a Ribosome Elongation Factor G Complex. J. Biol. Chem 2003, 278 (2), 1259–1267. [PubMed: 12409297]

(15). Hanson CL; Videler H; Santos C; Ballesta JPG; Robinson CV Mass Spectrometry of Ribosomes from Saccharomyces Cerevisiae: Implications for Assembly of the Stalk Complex. J. Biol. Chem 2004, 279 (41), 42750–42757. [PubMed: 15294894]

(16). Gordiyenko Y; Deroo S; Zhou M; Videler H; Robinson CV Acetylation of L12 Increases Interactions in the Escherichia Coli Ribosomal Stalk Complex. J. Mol. Biol 2008, 380 (2), 404–414. [PubMed: 18514735]

(17). Gordiyenko Y; Videler H; Zhou M; McKay AR; Fucini P; Biegel E; Müller V; Robinson CV Mass Spectrometry Defines the Stoichiometry of Ribosomal Stalk Complexes across the Phylogenetic Tree. Molecular & Cellular Proteomics 2010, 9 (8), 1774–1783. [PubMed: 20467040]

(18). Deroo S; Hyung S-J; Marcoux J; Gordiyenko Y; Koripella RK; Sanyal S; Robinson CV Mechanism and Rates of Exchange of L7/L12 between Ribosomes and the Effects of Binding EF-G. ACS Chem. Biol 2012, 7 (6), 1120–1127. [PubMed: 22489843]

(19). Fort KL; van de Waterbeemd M; Boll D; Reinhardt-Szyba M; Belov ME; Sasaki E; Zschoche R; Hilvert D; Makarov AA; Heck AJR Expanding the Structural Analysis Capabilities on an Orbitrap-Based Mass Spectrometer for Large Macromolecular Complexes. Analyst 2018, 143 (1), 100–105.

(20). van de Waterbeemd M; Fort KL; Boll D; Reinhardt-Szyba M; Routh A; Makarov A; Heck AJR High-Fidelity Mass Analysis Unveils Heterogeneity in Intact Ribosomal Particles. Nat. Methods 2017, 14 (3), 283–286. [PubMed: 28114288]

(21). van de Waterbeemd M; Tamara S; Fort KL; Damoc E; Franc V; Bieri P; Itten M; Makarov A; Ban N; Heck AJR Dissecting Ribosomal Particles throughout the Kingdoms of Life Using Advanced Hybrid Mass Spectrometry Methods. Nat. Commun 2018, 9 (1), 2493. [PubMed: 29950687]

(22). Lai S-H; Tamara S; Heck AJR Single-Particle Mass Analysis of Intact Ribosomes by Mass Photometry and Orbitrap-Based Charge Detection Mass Spectrometry. iScience 2021, 24 (11), 103211. [PubMed: 34712917]

(23). Smith LM; Kelleher NL Proteoform: A Single Term Describing Protein Complexity. Nat. Meth 2013, 10 (3), 186–187.

(24). Catherman AD; Skinner OS; Kelleher NL Top Down Proteomics: Facts and Perspectives. Biochem. Biophys. Res. Commun 2014, 445 (4), 683–693. [PubMed: 24556311]

(25). Brodbelt JS Deciphering Combinatorial Post-Translational Modifications by Top-down Mass Spectrometry. Curr. Opin. Chem. Biol 2022, 70, 102180. [PubMed: 35779351]

(26). Mehaffey MR; Xia Q; Brodbelt JS Uniting Native Capillary Electrophoresis and Multistage Ultraviolet Photodissociation Mass Spectrometry for Online Separation and Characterization of Escherichia Coli Ribosomal Proteins and Protein Complexes. Anal. Chem 2020, 92 (22), 15202–15211. [PubMed: 33156608]

(27). Strader MB; VerBerkmoes NC; Tabb DL; Connelly HM; Barton JW; Bruce BD; Pelletier DA; Davison BH; Hettich RL; Larimer FW; Hurst GB Characterization of the 70S Ribosome from Rhodopseudomonas Palustris Using an Integrated “Top-Down” and “Bottom-Up” Mass Spectrometric Approach. J. Proteome Res 2004, 3 (5), 965–978. [PubMed: 15473684]

(28). Zhang Y; Cai Q; Luo Y; Zhang Y; Li H Integrated Top-down and Bottom-up Proteomics Mass Spectrometry for the Characterization of Endogenous Ribosomal Protein Heterogeneity. Journal of Pharmaceutical Analysis 2023, 13 (1), 63–72. [PubMed: 36820077]

(29). Lermyte F; Tsybin YO; O’Connor PB; Loo JA Top or Middle? Up or Down? Toward a Standard Lexicon for Protein Top-Down and Allied Mass Spectrometry Approaches. J. Am. Soc. Mass Spectrom 2019, 30 (7), 1149–1157. [PubMed: 31073892]

Author Manuscript Author Manuscript Author Manuscript Author Manuscript

(30). Van Knippenberg P.h.; Hooykaas P. j. j.; Van Duin J The Stoichiometry of E. *Coli 30S Ribosomal Protein S1 on in Vivo and in Vitro Polyribosomes*, FEBS Letters 1974, 41 (2), 323–326. [PubMed: 4605341]

(31). Subramanian A-R Structure Qnd Functions of Ribosomal Protein S1. In Progress in Nucleic Acid Research and Molecular Biology; Cohn WE, Ed.; Academic Press, 1983; Vol. 28, pp 101–142 DOI: 10.1016/S0079-6603(08)60085-9. [PubMed: 6348874]

(32). Reier K; Lahtvee P-J; Liiv A; Remme J A Conundrum of R-Protein Stability: Unbalanced Stoichiometry of r-Proteins during Stationary Phase in Escherichia Coli. mBio 2022, 13 (5), No. e01873–22. [PubMed: 35980033]

(33). Crowe MC; Brodbelt JS Infrared Multiphoton Dissociation (IRMPD) and Collisionally Activated Dissociationof Peptides in a Quadrupole Ion Trapwith Selective IRMPD of Phosphopeptides. J. Am. Soc. Mass Spectrom 2004, 15 (11), 1581–1592. [PubMed: 15519225]

(34). Gardner MW; Li N; Ellington AD; Brodbelt JS Infrared Multiphoton Dissociation of Small-Interfering RNA Anions and Cations. J. Am. Soc. Mass Spectrom 2010, 21 (4), 580–591. [PubMed: 20129797]

(35). Madsen JA; Brodbelt JS Asymmetric Charge Partitioning upon Dissociation of DNA Duplexes. J. Am. Soc. Mass Spectrom 2010, 21 (7), 1144–1150. [PubMed: 20356762]

(36). Sciuto SV; Liu J; Konermann L An Electrostatic Charge Partitioning Model for the Dissociation of Protein Complexes in the Gas Phase. J. Am. Soc. Mass Spectrom 2011, 22 (10), DOI: 10.1007/s13361-011-0205-x.

(37). Pletnev PI; Nesterchuk MV; Rubtsova MP; Serebryakova MV; Dmitrieva K; Osterman IA; Bogdanov AA; Sergiev PV Oligoglutamylation of E. *Coli Ribosomal Protein S6 Is under Growth Phase Control*, Biochimie 2019, 167, 61–67. [PubMed: 31520657]

(38). Ramagopal S; Subramanian AR Alteration in the Acetylation Level of Ribosomal Protein L12 During Growth Cycle of Escherichia Coli. Proc. Natl. Acad. Sci. U.S.A 1974, 71 (5), 2136–2140. [PubMed: 4600787]

(39). Naganuma T; Nomura N; Yao M; Mochizuki M; Uchiumi T; Tanaka I Structural Basis for Translation Factor Recruitment to the Eukaryotic/Archaeal Ribosomes. J. Biol. Chem 2010, 285 (7), 4747–4756. [PubMed: 20007716]

(40). Helena-Bueno K; Rybak MY; Ekemezie CL; Sullivan R; Brown CR; Dingwall C; Baslé A; Schneider C; Connolly JPR; Blaza JN; Csörgő B; Moynihan PJ; Gagnon MG; Hill CH; Melnikov SV A New Family of Bacterial Ribosome Hibernation Factors. Nature 2024, 626 (8001), 1125–1132. [PubMed: 38355796]

Author Manuscript Author Manuscript Author Manuscript Author Manuscript

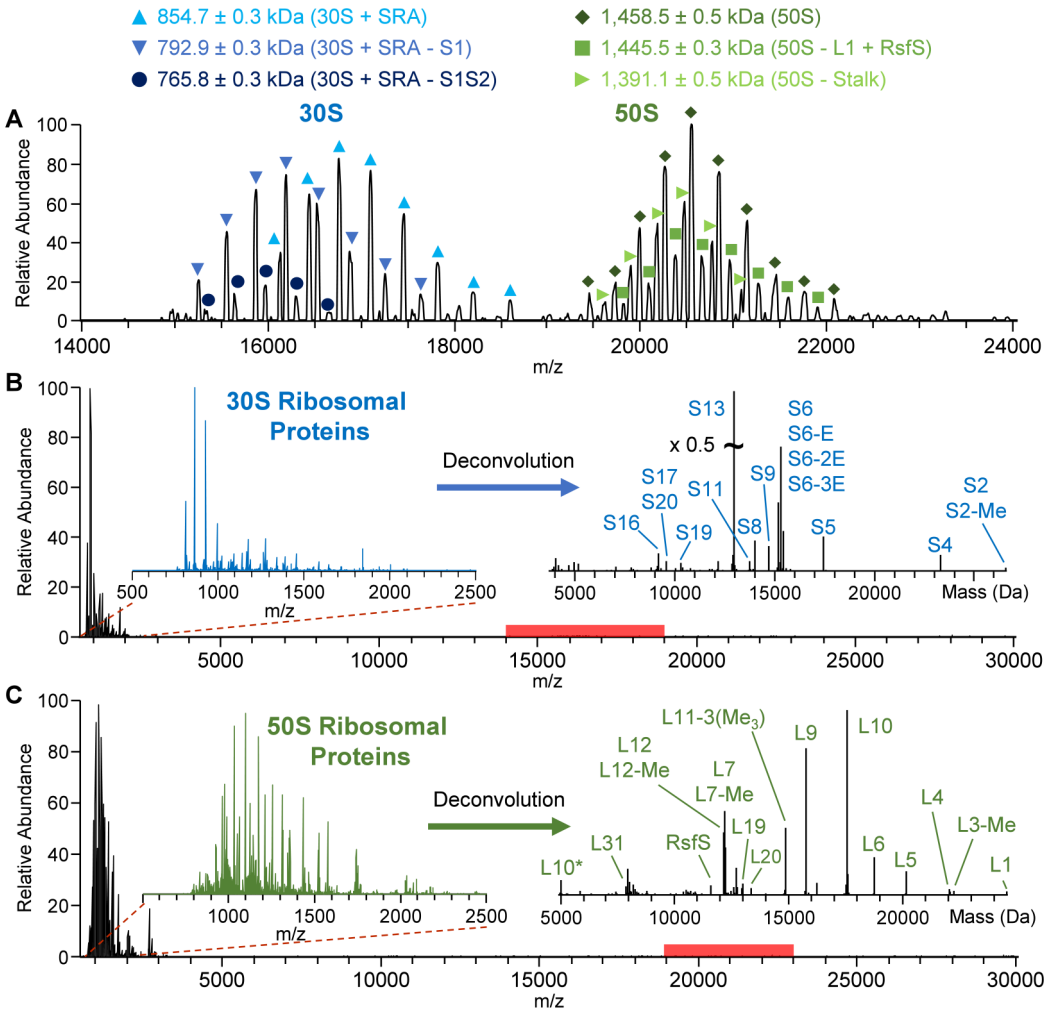

Figure 1.

Intact mass measurement of *E. coli* 30S and 50S ribosomal subunits (A). Masses are shown as the mean and standard deviation. Complex-up IRMPD spectra of 30S (B) and 50S (C) subunits with red boxes indicating the precursor *m*/*z* selection window. The inset spectra show zoomed-in regions of the IRMPD spectra containing intact RPs ejected from the subunits and charge deconvolved mass spectra with partial annotation.

Author Manuscript Author Manuscript Author Manuscript Author Manuscript

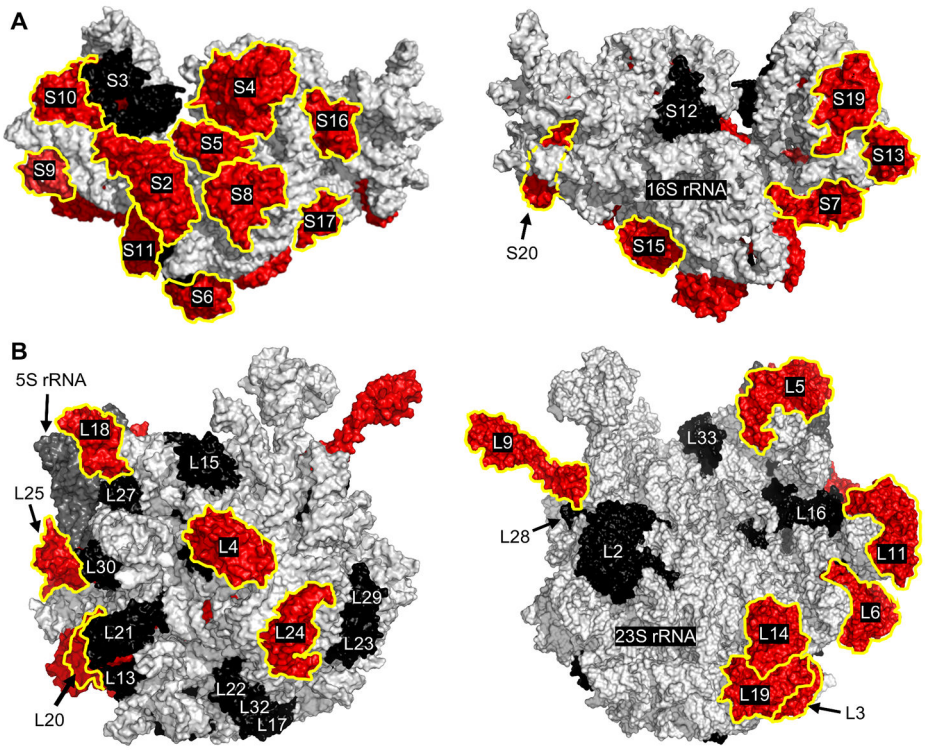

Figure 2.

Structures of *E. coli* 30S (A) and 50S (B) ribosomal subunits rotated 180° (left and right), based on structures 7OE1 and 6PJ6 and adapted using Pymol. RPs observed and not observed in the complex-up IRMPD analyses are highlighted in red and black, respectively, and rRNA is shown in gray. RPs L1, L7/L12, L10, and L31 were observed but are not present structures. RPs L34, L35, and L36 are buried within the folds of 23S rRNA.

Author Manuscript Author Manuscript Author Manuscript Author Manuscript

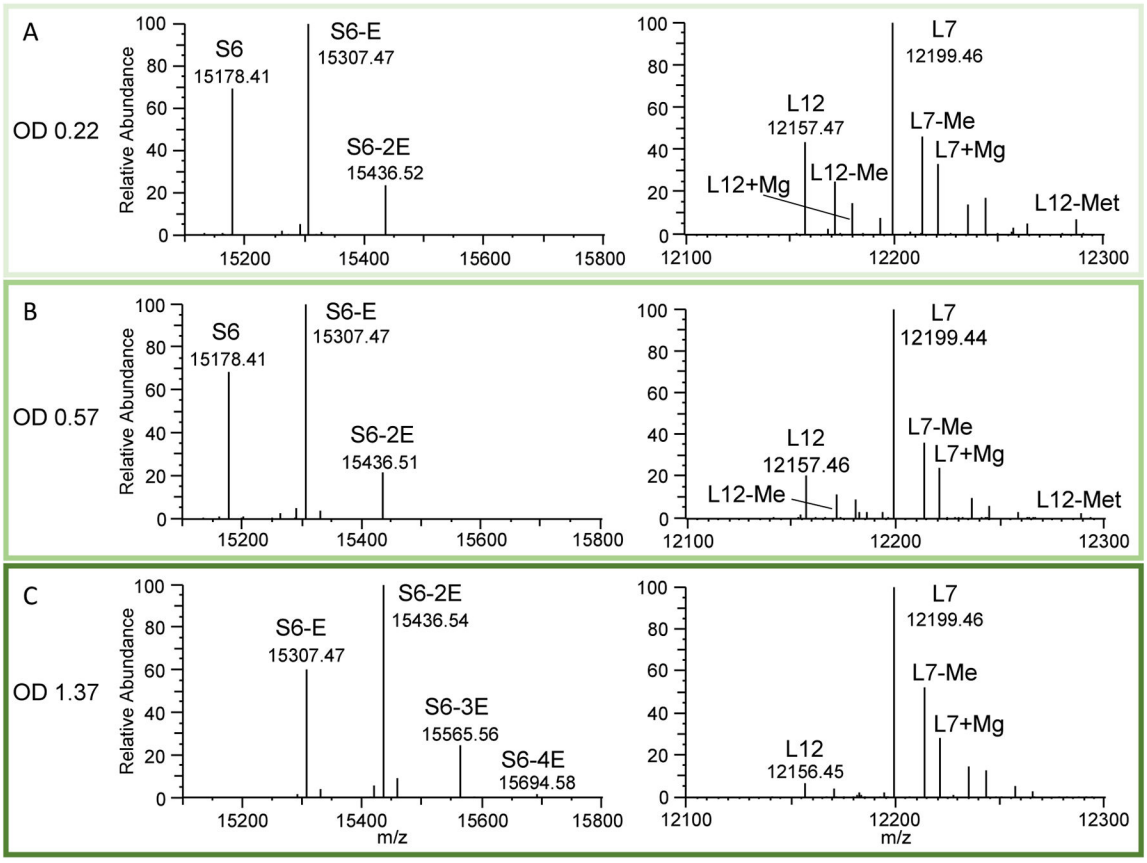

Figure 3.

Charge deconvolved complex-up IRMPD spectra of RPs S6 and L7/L12 demonstrating changes in proteoform abundance as a function of growth phase for ribosomes isolated from *E. coli* K12 cell cultures grown to OD_{600} values of 0.22 (A), 0.57 (B), and 1.37 (C). E indicates the number of C-terminal glutamylations, Me indicates lysine methylation, and Mg indicates a Mg^{2+}-bound species.

Author Manuscript Author Manuscript Author Manuscript Author Manuscript

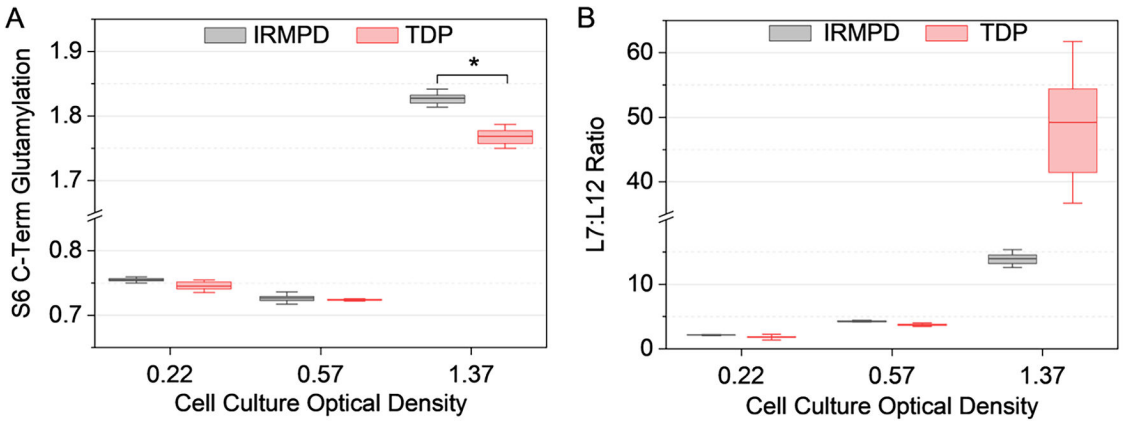

Figure 4.

Comparison of proteoform relative abundances determined by complex-up IRMPD and top-down proteomics (TDP) based on six replicate analyses for each approach. The number of S6 C-terminal glutamylations (A) and the stalk complex L7:L12 composition (B) for *E. coli* K12 ribosomes isolated from cultures with varying optical density at 600 nm. Boxes represent 25–75 percentile, and whiskers indicate 99% confidence intervals. *S6 glutamylation at 1.37 optical density is significantly different, but this is an artifact of low S/N of the tetra-glutamylation species in TDP precluding charge deconvolution.